CO_2 Reduction

DOI: 10.1002/anie.201310722

Rapid Selective Electrocatalytic Reduction of Carbon Dioxide to Formate by an Iridium Pincer Catalyst Immobilized on Carbon Nanotube Electrodes**

Peng Kang, Sheng Zhang, Thomas J. Meyer, and Maurice Brookhart**

Dedicated to the MPI für Kohlenforschung on the occasion of its centenary

Abstract: *An iridium pincer dihydride catalyst was immobilized on carbon nanotube-coated gas diffusion electrodes (GDEs) by using a non-covalent binding strategy. The as-prepared GDEs are efficient, selective, durable, gas permeable electrodes for electrocatalytic reduction of CO_2 to formate. High turnover numbers (ca. 54000) and turnover frequencies (ca. 15 s^{-1}) were enabled by the novel electrode architecture in aqueous solutions saturated in CO_2 with added HCO_3^-.*

Reduction of CO_2 to fuels and chemicals has attracted considerable attention as petroleum reserves dwindle.[1] Formic acid and formate are two-electron reduced products of CO_2 and can serve as hydrogen storage materials,[2] as precursors to methanol,[3] as reducing agents in organic synthesis,[4] as the fuel in fuel cell applications,[5] as an environmentally attractive substitute for mineral acids in applications in mining, drilling, and hydrofracking,[6] and as a feedstock for bacteria in the production of gasoline substitutes.[7] Currently, formic acid is produced by a multi-step chemical synthesis.[6a] Developing an efficient, single-step electrocatalytic method for formate/formic acid production could be of value in reducing cost,[8] thus enhancing their use in possible fuel cell and related applications.

Metal complexes and organometallic electrocatalysts are known for electrocatalytic CO_2 reduction[9] to formate[10] or CO[11] with high selectivity and efficiency. There is also extensive literature on CO_2 reduction at metal electrodes.[12] However, there are only limited reports of electrochemical reduction of CO_2 by supported organometallic catalysts,[13] even though this configuration is an important element in electrochemical and photoelectrochemical applications. Appealing in such applications is use of catalyst-loaded gas diffusion electrodes (GDEs), which can improve mass transport across the gas-liquid interface.[14] This application is particularly relevant to CO_2 reduction given its low solubility of about 30 mM in water.[12c,15] Utilization of the GDE configuration with surface-bound organometallic CO_2 reduction catalysts could significantly advance the utilization and integration of this family of catalysts in electrocatalysis.

Significant progress has been made in the functionalization of carbon surfaces by molecular attachment. Covalent immobilization strategies[13b,16] use covalent bonds to link to the surface, but they often require non-trivial pre-treatment of the carbon surface. Non-covalent surface binding methods use strong van der Waals π–π interactions between polyaromatic hydrocarbons and graphitized carbon surfaces. They offer a convenient, non-destructive approach to catalyst immobilization, which can result in excellent surface stability.[16a] This approach has been used to surface-bind water oxidation,[17] proton reduction,[18] and, recently, CO_2 reduction catalysts for electrocatalytic reduction to CO.[19] We report herein the application of this approach to electrocatalytic CO_2 reduction to formate in a gas diffusion electrode with notable rates, turnover numbers, and surface stability.

We previously reported homogeneous electrochemical reduction of CO_2 to formate in both non-aqueous and aqueous media with Ir pincer dihydride complexes.[10d,e] The Ir catalysts are efficient and highly selective in generating formate without catalyzing the reduction of CO_2 to CO and water to H_2. Herein we immobilize a pyrene-modified Ir pincer dihydride complex, **1**, onto large-surface-area, multi-walled carbon nanotube (CNT) coated gas diffusion electrodes (Scheme 1). The resulting derivatized electrodes exhibit impressive rates and turnover numbers for the electrochemical reduction of CO_2 to formate.

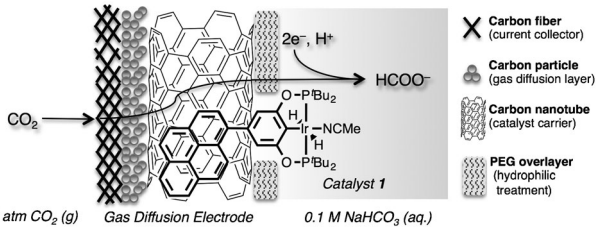

Scheme 1. Illustration of a carbon nanotube-coated gas diffusion electrode with surface-bound Ir pincer dihydride catalyst **1** for electrochemical reduction of CO_2 to formate.

[*] Dr. P. Kang, Dr. S. Zhang, Prof. T. J. Meyer, Prof. M. Brookhart
Department of Chemistry
The University of North Carolina at Chapel Hill
Chapel Hill, NC 27599 (USA)
E-mail: tjmeyer@unc.edu
mbrookhart@unc.edu

[**] We gratefully acknowledge the financial support from the UNC EFRC: Center for Solar Fuels, an Energy Frontier Research Center funded by the U.S. Department of Energy Office of Science, Office of Basic Energy Sciences under Award Number DE-SC0001011. A provisional patent application based on this work has been filed with USPTO.

Supporting information for this article is available on the WWW under http://dx.doi.org/10.1002/anie.201310722.

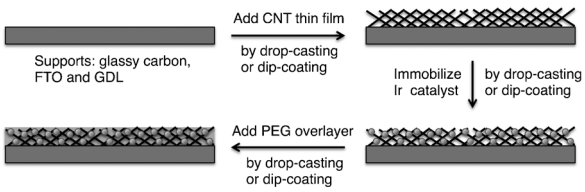

Scheme 2. Fabrication of Ir catalyst-loaded carbon nanotube electrodes (FTO = fluorine doped tin oxide, GDL = gas-diffusion layer; see the Supporting Information for details).

Nanostructured electrodes were prepared as visualized in Scheme 2. The CNTs were ultrasonically dispersed in DMF (1 mg mL^{-1}) without use of a surfactant. Support electrodes, glassy carbon (GC) or fluorine-doped tin oxide (FTO), were drop-cast with the CNT suspension (ca. 0.03 mg cm^{-2} coverage). The morphology of deposited CNT thin film on FTO was shown by scanning electron microscopy (SEM) to be a highly porous nanostructure (Figure 1 a,b). No bare FTO

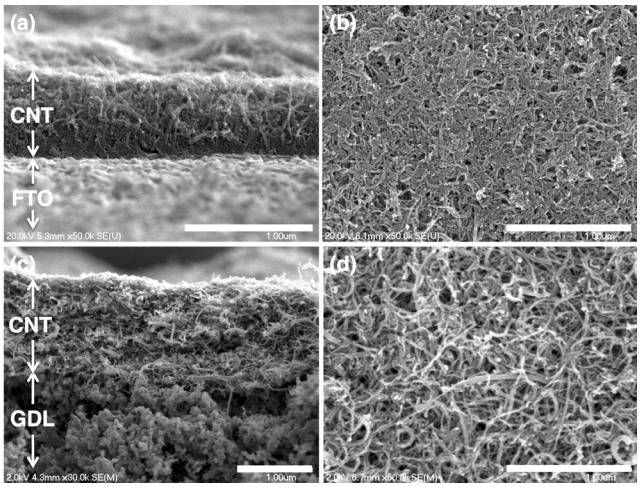

Figure 1. SEM images of CNT thin films on FTO (a, b) and GDL (c, d). Left: cross-section; right: top view. Scale bar: 1 μm.

surface was observed. The average film thickness was measured as 500–700 nm and the pore size between 20–100 nm. The electroactive surface area of an as-made GC/CNT electrode was estimated by cyclic voltammetry (CV) with $[Fe(CN)_6]^{3-/4-}$ as the probe couple. The measured surface area was about five times higher than the bare GC electrode (Supporting Information, Figure S2). The high porosity and increased electroactive surface area provide a basis for achieving high current densities in CO_2 electrolyses.

The iridium pincer dihydride complex **1** (Scheme 1) was immobilized by drop-casting a MeCN solution (0.2 mM) on CNT coated GC or FTO electrodes under Ar (Scheme 2). X-ray photoelectron spectroscopy (XPS) of the FTO/CNT/**1** electrode exhibited Ir $4f_{5/2}$ and $4f_{7/2}$ peaks at 62.1 and 64.5 eV and a P 2p peak at 132.3 eV with an Ir/P ratio of about 1:1.8 (Supporting Information, Figure S14, Table S1). A polyethylene glycol (PEG) overlayer (ca. 3 μg cm^{-2}) was subsequently applied by drop-casting 0.01 % w/w aq. solution onto the GC/CNT/**1** electrode. The PEG overlayer does not affect the electroactive surface area significantly, but it does render the CNT surface hydrophilic. In water, the PEG layer remains attached to the CNT surface owing to strong non-covalent interactions.[16a,20]

The response of the GC/CNT/**1**/PEG electrode under Ar in water (0.1 M $NaHCO_3$, 0.5 M $LiClO_4$, 1 % MeCN v/v) was probed by cyclic voltammetry (CV). A reduction wave with peak potential at $E_{p,c} = -1.25$ V vs NHE ($E_{p,c}$, the cathodic peak potential) was observed (Figure 2, left) along with

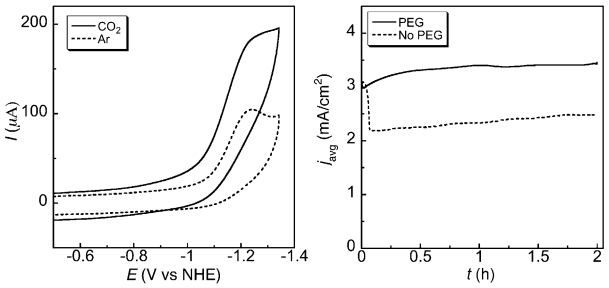

Figure 2. Left: Cyclic voltammograms (CVs) of a GC/CNT/**1**/PEG electrode in water, under Ar (dotted) and 1 atm CO_2 (solid) at 100 mV s^{-1} scan rate. Right: Controlled potential electrolyses with GC/CNT/**1**/PEG (——; Table 1, entry 3) and GC/CNT/**1** electrodes (••••; Table 1, entry 6) in water under 1 atm CO_2. Conditions: 0.1 M $NaHCO_3$, 0.5 M $LiClO_3$, 1 % v/v MeCN, electrode area 0.072 cm^2, room temperature.

oxidation waves with peak potentials at $E_{p,a} = 0.15$ and 0.30 V ($E_{p,a}$, the anodic peak potential) on a reverse scan (Supporting Information, Figure S4). Consistent with previous studies in solution,[10e] the reduction wave arises from formation of **1** by 2 e$^-$/1 H$^+$ reduction, and the oxidation waves from re-oxidation of **1** by 2 e$^-$/1 H$^+$ to cation **2** (Scheme 3). Variations in peak current ($i_{p,c}$) for the reduction wave at $E_{p,c} = -1.25$ V are proportional to the scan rate v, which is characteristic of

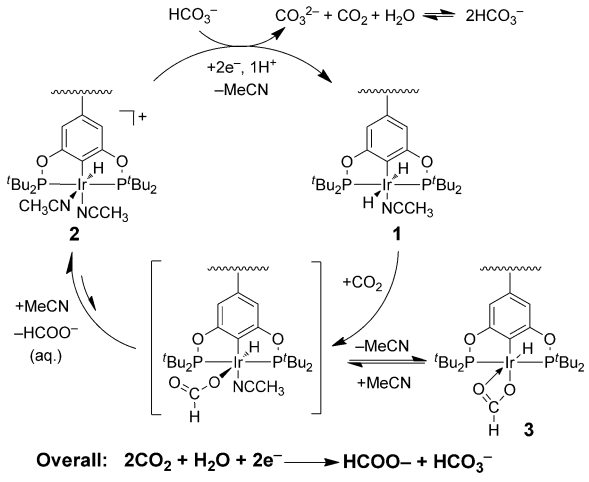

Scheme 3. Proposed mechanism for interfacial reduction of CO_2 to formate.

a redox response from a surface-immobilized redox entity [Eq. (1); Supporting Information, Figure S3].

$$i_{p,c} = (n^2 F^2 v A \Gamma)/(4RT) \quad (1)$$

In Equation (1), Γ is the surface coverage [mol cm^{-2}], Q is the charge under the surface wave [C], v the scan rate [V s^{-1}], F the Faradaic constant, A the electrode area [cm^2], and n is the number of electrons transferred. The surface coverage was calculated from Equation (2) with charge Q obtained by

$$\Gamma = Q/nFA \quad (2)$$

integration of the reduction wave. With $n = 2$,[10e] a typical coverage on a GC/CNT electrode was calculated to be $\Gamma = 2.2 \times 10^{-9}$ mol cm^{-2}.

Under 1 atm of CO_2, the reduction wave at $E_{p,c} = -1.25$ V was catalytically enhanced with an onset at about -1.05 V (Figure 2, left). Current enhancements by a factor of about two were observed at a scan rate of 100 mV s^{-1}. The activation overpotential[21] is about 0.55 V based on $E^0 = -0.49$ V for CO_2 reduction to formate at pH 7.[9g] Between scan rates from 100 to 500 mV s^{-1}, catalytic currents were not linearly varied with scan rates (Supporting Information, Figure S5), suggesting that the rate of electrocatalysis is largely dictated by a rate-limiting chemical step. In this limit, the catalytic current, i_{cat}, is related to the catalytic rate constant, k_{cat}, or turnover frequency TOF, as shown in Equation (3).

$$i_{cat} = n_{cat} F A \Gamma k_{cat} \quad (3)$$

Using $n_{cat} = 2$ for formate production, k_{cat} was calculated as 6.7 s^{-1}. This value is comparable to k_{cat} of 7.3 s^{-1} for the related water-soluble Ir pincer catalyst reported previously.[10e] The slope of a Tafel plot of log j (j = current density) as a function of overpotential was measured as 192 mV/dec under steady-state conditions (Supporting Information, Figure S10). Transfer coefficient α was calculated as 0.31 and exchange current density j_0 as 4.5×10^{-6} mA cm^{-2}. No significant change was observed in the catalytic current with variations in the $NaHCO_3$ concentration between 0.1 and 0.5 M with the ionic strength held constant at 0.6 M (Supporting Information, Figure S11).

The Ir pincer catalyst exhibits high surface stability under catalytic conditions. The derivatized surface retained its electrochemical response after soaking in water under Ar for a day. The catalytic current under CO_2 was cycled 50 times with less than a 10% drop in current (Supporting Information, Figure S8). Surface stability in this case arises largely from π–π interactions between the pyrene linker and the CNT surface. The π–π interaction between a single pyrene and sp^2 carbon surfaces has been estimated as 9.1 kcal mol^{-1}.[22] Additional surface stability is derived from the four *tert*-butyl groups of the catalyst rendering it highly hydrophobic and insoluble in water. The two factors combine to create a high degree of stability of the catalyst on the surface even without a covalent linker.

Long-term electrolyses were performed in aqueous media under a variety of conditions (Table 1). With GC/CNT/**1**/PEG electrodes (entries 1–3), currents were sustained during the electrolyses (Figure 2, right) with current densities ranging from 1–3.3 mA cm^{-2} with the pH held constant at 6.8. Faradaic efficiencies for formate production were generally above 90% and up to 96%, as shown in entry 1. The only product in the headspace was H_2 with no CO observed by GC analyses. Decreasing the applied potential from -1.2 V to -1.3 and -1.4 V (Table 1, entries 1–3) increases the current density from 1.0 to 3.3 mA cm^{-2} but also slightly increases H_2 formation. In the absence of the Ir catalyst (entry 5), the GC/CNT/PEG electrode generates predominantly H_2 (90%). This observation points to H_2 production in entries 1–3 as a background reaction at the CNT electrode.

The efficiency of the surface catalytic system is remarkable. The maximum turnover frequency (TOF) under 1 atm of CO_2 based on formate production was 7.4 s^{-1} (Table 1, entry 3). The catalyst exhibited high stability in the bulk electrolyses, leading to high turnover numbers (TON). Electrolysis over an eight-hour period (Table 1, entry 4) produces formate to a concentration of about 11 mM in water with a TON of 203 000, highlighting the high efficiency and longevity of this system.

Sustained catalysis requires addition of small amounts of MeCN and the PEG overlayer. Addition of 1% v/v MeCN stabilizes cationic species **2**, as noted in the earlier study in water.[10e] The PEG overlayer is critical for stabilizing the catalytic interface. Without this overlayer, the catalytic current dropped during the initial 5 min of the electrolysis

Table 1: Conditions for controlled-potential electrolysis and product analyses.[a]

Entry	Cathode	E [V vs NHE]	j_{avg} [mA cm^{-2}]	t [h]	$HCOO^-$ Yield [%][b]	$HCOO^-$ TON	$HCOO^-$ TOF [s^{-1}]	H_2 Yield [%][c]	CO Yield [%][c]
1	GC/CNT/**1**/PEG[d]	−1.2	1.0	2	96	16 000	2.3	3	n.o.[e]
2	GC/CNT/**1**/PEG[d]	−1.3	2.2	2	94	35 000	4.9	4	n.o.[e]
3	GC/CNT/**1**/PEG[d]	−1.4	3.3	2	93	53 000	7.4	7	n.o.[e]
4	GC/CNT/**1**/PEG[d]	−1.4	3.6	8	83	203 000	7.0	12	n.o.[e]
5	GC/CNT/PEG[d]	−1.4	1.7	2	5	1500	0.2	90	2
6	GC/CNT/**1**[d]	−1.4	2.3	2	89	33 000	4.6	10	n.o.[e]
7	GDL/CNT/**1**/PEG[f]	−1.4	15.6	1	83	54 200	15.1	[g]	[g]

[a] Conditions: 0.5 M $LiClO_4$, 0.1 M $NaHCO_3$, 1% v/v MeCN, 1 atm CO_2, SCE reference electrode, Pt mesh counter electrode. [b] Analyzed by ^{1}H NMR spectroscopy. [c] Analyzed by GC. [d] Electrode area = 0.07 cm^2. [e] Not observed. [f] With the gas diffusion electrode in Scheme 1; CO_2 flow rate = 0.8 L min^{-1}, electrode area = 1.5 cm^2. [g] Gaseous product not determined owing to CO_2 purging.

to about 60% of the initial current density, leading to lower current density (Figure 2, right; Table 1, entry 6). A CV scan afterward showed a new, single oxidation wave at $E_{p,a} = 0.40$ V versus NHE (Supporting Information, Figure S6), consistent with the oxidation wave from the authentic neutral formate complex **3** (Supporting Information, Figure S7) in Scheme 3, which was not observed with the added PEG overlayer.

Sustained catalysis requires access of water to the catalyst for formate dissociation, solvation, and regeneration of **2**, as shown in the mechanism in Scheme 3. The CNT surface is hydrophobic, as observed visually by the high contact angle for water droplets on the surface. Without the PEG overlayer, retention of formate in the coordination sphere stabilizes and deactivates the catalyst as the formate complex **3** (Scheme 3). With added PEG overlayer, the CNT surface is rendered more hydrophilic, and formate is solvolyzed and rapidly released to the external solution, regenerating electroactive **2**.

The non-covalent immobilization strategy enables the CNT electrode to be readily replenished with fresh Ir catalyst for reuse. The iridium catalyst can be removed by soaking the electrode in THF, leaving a clean electrode surface with essentially no electrochemical response under CO_2. Newly prepared catalyst solutions can be re-deposited by using the procedure in Scheme 2. Renewed electrodes show no significant reduction in surface coverage over five cycles of loading/deloading (Supporting Information, Figure S9). The CNT film also exhibits excellent mechanical stability, with no visible peeling after multiple catalytic cycles.

Non-covalent surface binding was used to fabricate large-surface-area gas diffusion electrodes (GDEs). A carbon fiber paper with a carbon black gas diffusion layer was dip-coated by using a CNT DMF suspension (Scheme 2, ca. 0.06 mg cm^{-2} CNT coverage) and characterized by SEM. The cross-section images show a stacked triple-layer (Figure 1c; Supporting Information, Figure S9): a carbon fiber macroporous layer (240 μm thick), a carbon black microporous layer (50 μm), and a CNT nanoporous layer (1.2 μm). The CNT film morphology and porosity are comparable with those on FTO, but with nearly doubled thicknesses (Figure 1c,d). The catalyst **1** and PEG overlayer were sequentially applied using dip-coating (Scheme 2). XPS showed comparable Ir/C ratios with those on FTO (Supporting Information, Figure S15 and Table S1). Using the Ir/C ratio and the CNT coverage, the catalyst loading on the GDE was estimated to be 3.8×10^{-9} mol cm^{-2} (Supporting Information).

Use of the GDE resulted in significantly enhanced current densities while retaining excellent formate selectivity. With the configuration in Scheme 1, the current density was further increased to 15.6 mA cm^{-2} (Table 1, entry 7), compared to 3.3 mA cm^{-2} with a disk electrode (entry 3). The formate selectivity was about 83% and the current was stable for over 1 hour. The circa five-fold further increase in current density presumably originates from an optimized structure and proper configuration of the GDE. The triple-layered structure with the PEG overlayer in the GDE appears to offer beneficial partitioning between hydrophobic and hydrophilic regions, leading to an increase in the gas–liquid interface facilitating CO_2 transport. When the GDE interfaces both gas and aqueous phases, the Ir catalyst can access sufficient CO_2 from the gas phase and readily release formate to the aqueous phase, relieving mass transport constraints. Further increases in the current density are expected in a microflow reactor.[12c]

In summary, the pyrene-modified iridium pincer dihydride catalyst **1** has been immobilized on carbon nanotube-coated gas diffusion electrodes by using a non-covalent approach. The supported Ir catalyst exhibits notable efficiency, selectivity, and longevity for the electrochemical production of formate from CO_2. Optimization with a gas diffusion electrode modified with the Ir catalyst gives current densities up to about 15 mA cm^{-2}, and maintains high formate selectivity; however, integration of this electrode into a practical electrolysis device will require further advances. The architecture of the gas diffusion electrode with an anchored molecular catalyst is novel and the method of catalyst incorporation generic, with potential for broad applications.

Received: December 10, 2013
Revised: April 29, 2014
Published online: June 4, 2014

Keywords: carbon dioxide · electrochemistry · formate · gas diffusion electrodes · iridium

[1] *Climate Change: Evidence, Impacts, and Choices: Set of 3 Booklets*, The National Academies Press, New York, **2012**.
[2] T. C. Johnson, D. J. Morris, M. Wills, *Chem. Soc. Rev.* **2010**, *39*, 81–88.
[3] C. A. Huff, M. S. Sanford, *J. Am. Chem. Soc.* **2011**, *133*, 18122–18125.
[4] R. Noyori, S. Hashiguchi, *Acc. Chem. Res.* **1997**, *30*, 97–102.
[5] C. Rice, R. I. Ha, R. I. Masel, P. Waszczuk, A. Wieckowski, T. Barnard, *J. Power Sources* **2002**, *111*, 83–89.
[6] a) W. Reutemann, H. Kieczka in *Ullmann's Encyclopedia of Industrial Chemistry*, Wiley-VCH, Weinheim, **2000**; b) A. J. S. Pollard, D. S. Banasiak, C. J. Ellens, J. N. Brown (Avello Bioenergy, Inc.), United States Patent Application 20120302470, **2012**.
[7] H. Li, P. H. Opgenorth, D. G. Wernick, S. Rogers, T. Y. Wu, W. Higashide, P. Malati, Y. X. Huo, K. M. Cho, J. C. Liao, *Science* **2012**, *335*, 1596–1596.
[8] A. S. Agarwal, Y. M. Zhai, D. Hill, N. Sridhar, *ChemSusChem* **2011**, *4*, 1301–1310.
[9] a) E. E. Benson, C. P. Kubiak, A. J. Sathrum, J. M. Smieja, *Chem. Soc. Rev.* **2009**, *38*, 89–99; b) M. Cokoja, C. Bruckmeier, B. Rieger, W. A. Herrmann, F. E. Kuhn, *Angew. Chem.* **2011**, *123*, 8662–8690; *Angew. Chem. Int. Ed.* **2011**, *50*, 8510–8537; c) C. Finn, S. Schnittger, L. J. Yellowlees, J. B. Love, *Chem. Commun.* **2012**, *48*, 1392–1399; d) A. M. Appel, J. E. Bercaw, A. B. Bocarsly, H. Dobbek, D. L. DuBois, M. Dupuis, J. G. Ferry, E. Fujita, R. Hille, P. J. A. Kenis, C. A. Kerfeld, R. H. Morris, C. H. F. Peden, A. R. Portis, S. W. Ragsdale, T. B. Rauchfuss, J. N. H. Reek, L. C. Seefeldt, R. K. Thauer, G. L. Waldrop, *Chem. Rev.* **2013**, *113*, 6621–6658; e) C. Costentin, M. Robert, J.-M. Saveant, *Chem. Soc. Rev.* **2013**, *42*, 2423–2436; f) P. Kang, Z. Chen, M. Brookhart, T. J. Meyer, *Top. Catal.* **2014**, accepted; g) M. D. Doherty, D. C. Grills, J. T. Muckerman, D. E. Polyansky, E. Fujita, *Coord. Chem. Rev.* **2010**, *254*, 2472–2482.
[10] a) H. Ishida, H. Tanaka, K. Tanaka, T. Tanaka, *J. Chem. Soc. Chem. Commun.* **1987**, 131–132; b) C. Arana, S. Yan, M. Keshavarzk, K. T. Potts, H. D. Abruna, *Inorg. Chem.* **1992**, *31*, 3680–3682; c) C. Caix, S. Chardon-Noblat, A. Deronzier, *J.*

Electroanal. Chem. **1997**, *434*, 163 – 170; d) P. Kang, C. Cheng, Z. F. Chen, C. K. Schauer, T. J. Meyer, M. Brookhart, *J. Am. Chem. Soc.* **2012**, *134*, 5500 – 5503; e) P. Kang, T. J. Meyer, M. Brookhart, *Chem. Sci.* **2013**, *4*, 3497 – 3502.

[11] a) J. Hawecker, J. M. Lehn, R. Ziessel, *J. Chem. Soc. Chem. Commun.* **1984**, 328 – 330; b) M. Beley, J. P. Collin, R. Ruppert, J. P. Sauvage, *J. Chem. Soc. Chem. Commun.* **1984**, 1315 – 1316; c) J. M. Smieja, C. P. Kubiak, *Inorg. Chem.* **2010**, *49*, 9283 – 9289; d) M. Bourrez, F. Molton, S. Chardon-Noblat, A. Deronzier, *Angew. Chem.* **2011**, *123*, 10077 – 10080; *Angew. Chem. Int. Ed.* **2011**, *50*, 9903 – 9906; e) Z. F. Chen, C. C. Chen, D. R. Weinberg, P. Kang, J. J. Concepcion, D. P. Harrison, M. S. Brookhart, T. J. Meyer, *Chem. Commun.* **2011**, *47*, 12607 – 12609; f) C. Costentin, S. Drouet, M. Robert, J.-M. Saveant, *Science* **2012**, *338*, 90 – 94; g) V. S. Thoi, N. Kornienko, C. G. Margarit, P. Yang, C. J. Chang, *J. Am. Chem. Soc.* **2013**, *135*, 14413 – 14424.

[12] a) Y. Hori, H. Wakebe, T. Tsukamoto, O. Koga, *Electrochim. Acta* **1994**, *39*, 1833 – 1839; b) Y. H. Chen, M. W. Kanan, *J. Am. Chem. Soc.* **2012**, *134*, 1986 – 1989; c) C. Delacourt, P. L. Ridgway, J. B. Kerr, J. Newman, *J. Electrochem. Soc.* **2008**, *155*, B42 – B49; d) B. A. Rosen, A. Salehi-Khojin, M. R. Thorson, W. Zhu, D. T. Whipple, P. J. A. Kenis, R. I. Masel, *Science* **2011**, *334*, 643 – 644; e) S. Zhang, P. Kang, T. J. Meyer, *J. Am. Chem. Soc.* **2014**, *136*, 1734 – 1737.

[13] a) S. Chardon-Noblat, A. Deronzier, R. Ziessel, D. Zsoldos, *J. Electroanal. Chem.* **1998**, *444*, 253 – 260; b) S. A. Yao, R. E. Ruther, L. Zhang, R. A. Franking, R. J. Hamers, J. F. Berry, *J. Am. Chem. Soc.* **2012**, *134*, 15632 – 15635.

[14] a) R. Borup, J. Meyers, B. Pivovar, Y. S. Kim, R. Mukundan, N. Garland, D. Myers, M. Wilson, F. Garzon, D. Wood, P. Zelenay, K. More, K. Stroh, T. Zawodzinski, J. Boncella, J. E. McGrath, M. Inaba, K. Miyatake, M. Hori, K. Ota, Z. Ogumi, S. Miyata, A. Nishikata, Z. Siroma, Y. Uchimoto, K. Yasuda, K. I. Kimijima, N. Iwashita, *Chem. Rev.* **2007**, *107*, 3904 – 3951; b) L. Cindrella, A. M. Kannan, J. F. Lin, K. Saminathan, Y. Ho, C. W. Lin, J. Wertz, *J. Power Sources* **2009**, *194*, 146 – 160.

[15] H. R. Jhong, F. R. Brushett, P. J. A. Kenis, *Adv. Energy Mater.* **2013**, *3*, 589 – 599.

[16] a) D. Tasis, N. Tagmatarchis, A. Bianco, M. Prato, *Chem. Rev.* **2006**, *106*, 1105 – 1136; b) C. C. L. McCrory, A. Devadoss, X. Ottenwaelder, R. D. Lowe, T. D. P. Stack, C. E. D. Chidsey, *J. Am. Chem. Soc.* **2011**, *133*, 3696 – 3699; c) E. C. Landis, R. J. Hamers, *Chem. Mater.* **2009**, *21*, 724 – 730; d) M. V. Sheridan, K. Lam, W. E. Geiger, *J. Am. Chem. Soc.* **2013**, *135*, 2939 – 2942.

[17] F. Li, B. B. Zhang, X. N. Li, Y. Jiang, L. Chen, Y. Q. Li, L. C. Sun, *Angew. Chem.* **2011**, *123*, 12484 – 12487; *Angew. Chem. Int. Ed.* **2011**, *50*, 12276 – 12279.

[18] P. D. Tran, A. Le Goff, J. Heidkamp, B. Jousselme, N. Guillet, S. Palacin, H. Dau, M. Fontecave, V. Artero, *Angew. Chem.* **2011**, *123*, 1407 – 1410; *Angew. Chem. Int. Ed.* **2011**, *50*, 1371 – 1374.

[19] J. D. Blakemore, A. Gupta, J. J. Warren, B. S. Brunschwig, H. B. Gray, *J. Am. Chem. Soc.* **2013**, *135*, 18288 – 18291.

[20] R. Shvartzman-Cohen, Y. Levi-Kalisman, E. Nativ-Roth, R. Yerushalmi-Rozen, *Langmuir* **2004**, *20*, 6085 – 6088.

[21] Activation overpotential is the difference between the thermodynamic potential and the catalytic onset potential, but does not include additional factors influencing the applied overvoltage (ca. 0.15–0.35 V; see Table 1).

[22] J. A. Mann, J. Rodriguez-Lopez, H. D. Abruna, W. R. Dichtel, *J. Am. Chem. Soc.* **2011**, *133*, 17614 – 17617.

